Disassembling 2D van der Waals Crystals into Macroscopic Monolayers and Reassembling into Artificial Lattices

Fang Liu¹, Wenjing Wu¹, Yusong Bai¹, Sang Hoon Chae², Qiuyang Li¹, Jue Wang¹, James Hone², X.-Y. Zhu^{1,*}

Abstract

Two-dimensional materials from layered van der Waals (vdW) crystals hold great promises for electronic, optoelectronic, and quantum devices, but technological implementation will be hampered by the lack of high-throughput techniques for exfoliating single crystal monolayers with sufficient size and high quality. Here we report a facile method to disassemble vdW single crystals layer-by-layer into monolayers with near-unity yield and with dimensions limited only by bulk crystal sizes. The macroscopic monolayers are comparable in quality to microscopic monolayers from conventional Scotch tape exfoliation. The monolayers can be assembled into macroscopic artificial structures, including TMDC multilayers with broken inversion symmetry and dramatically enhanced nonlinear optical response. This approach takes us one step closer to mass production of macroscopic monolayers and bulk-like artificial materials with controllable properties.

Since the first report of monolayer graphene in 2004,(I) studies of 2D materials have grown into one of the most active research fields today.(2) Monolayers, and especially their homo- or hetero-structures have been excellent playgrounds for the exploration of new physical phenomena and hold great promises for next generation devices, particularly quantum devices.(3-5) Many of these novel quantum phenomena, such as moiré excitons in transition metal dichalcogenides (TMDC) heterobilayers and superconductivity in twisted bilayer graphene, rely on monolayers with single crystal lattices.(3-12) However, despite extensive advances in research, the absence of

¹ Department of Chemistry, Columbia University, New York, NY 10027, USA

² Department of Mechanical Engineering, Columbia University, New York, NY 10027, USA

^{*} To whom correspondence should be addressed. Email: xyzhu@columbia.edu

high throughput methods to produce high quality 2D single crystals with macroscopic sizes remains as a major challenge for their mass production and potential commercialization. Past attempts of producing 2D monolayers are often limited among several crucial aspects, such as material quality, scalability, and sizes. Liquid phase exfoliation is scalable, but generates small sizes (few µm) and poor quality.(13) Chemical vapor deposition (CVD) can grow continuous monolayers on wafer scales, albeit in the polycrystalline form with high defect density, thereby limiting their performance in electronic devices. (14) Mechanical exfoliation, utilizing the famous Scotch-tape method, (I) so far produces the highest quality monolayers; however, the typical lateral dimensions is <100 μm, with very low yield. Larger flakes can be obtained using metals with stronger vdW adhesion to 2D materials than interlayer vdW force, as demonstrated for TMDCs. Exfoliation of bulk TMDC crystals on gold substrates has been reported to yield monolayers up to cm scale, (15, 16) but it is difficult to remove the TMDC monolayers from the gold substrate. Another strategy involves evaporation of metal onto the surface of a bulk TMDC crystal, followed by exfoliation, transferring onto a desired substrate, and chemical etching. (17, 18) This method have been demonstrated to yield single crystal TMDC monolayers up to 500 µm in lateral dimensions(17) and transfer CVD films up to wafer scale(18). However, direct deposition of metal onto TMDC bulk crystal introduces significant defects in the TMDC monolayer. (19)

Here we demonstrate a non-destructive, high throughput, and widely applicable technique to disassemble 2D vdW crystals layer-by-layer into single crystal monolayers, with near unity yield. This method works for a range of vdW materials and generates monolayers with macroscopic dimensions limited only by the sizes of the bulk crystals. As schematically shown in Fig. 1a, a critical step is obtaining an atomically flat gold tape, i.e., ultra-flat gold film on a polymer substrate, achieved with a template-stripping technique.(20, 21) Following evaporation of a thin gold film on an ultra-flat surface of highly polished silicon wafer, the gold film is stripped off the substrate with thermal release tape and a polyvinylpyrrolidone (PVP) interfacial layer. The exposed Au surface is templated by the flat substrate with roughness on the Å scale.(20, 21) The ultra-flat gold tape allows intimate and uniform vdW contact between the gold and a 2D vdW crystal surface, exfoliating a complete monolayer, which can be transferred onto the desired substrate. After removing the thermal release tape, washing off the PVP layer, and etching of Au with a mild etchant solution (I₂/I⁻), a monolayer with macroscopic dimension (typically mm to cm) is obtained. In addition to increasing the lateral sizes and monolayer yields by 2-3 orders of magnitude, our Au

tape exfoliation turns the *stochastic* Scotch tape method into a *deterministic* and *quantitative* process. Although Au is used in the present study, one can extend the method to other metals as long as the etching chemistry does not damage the 2D monolayer of interest.

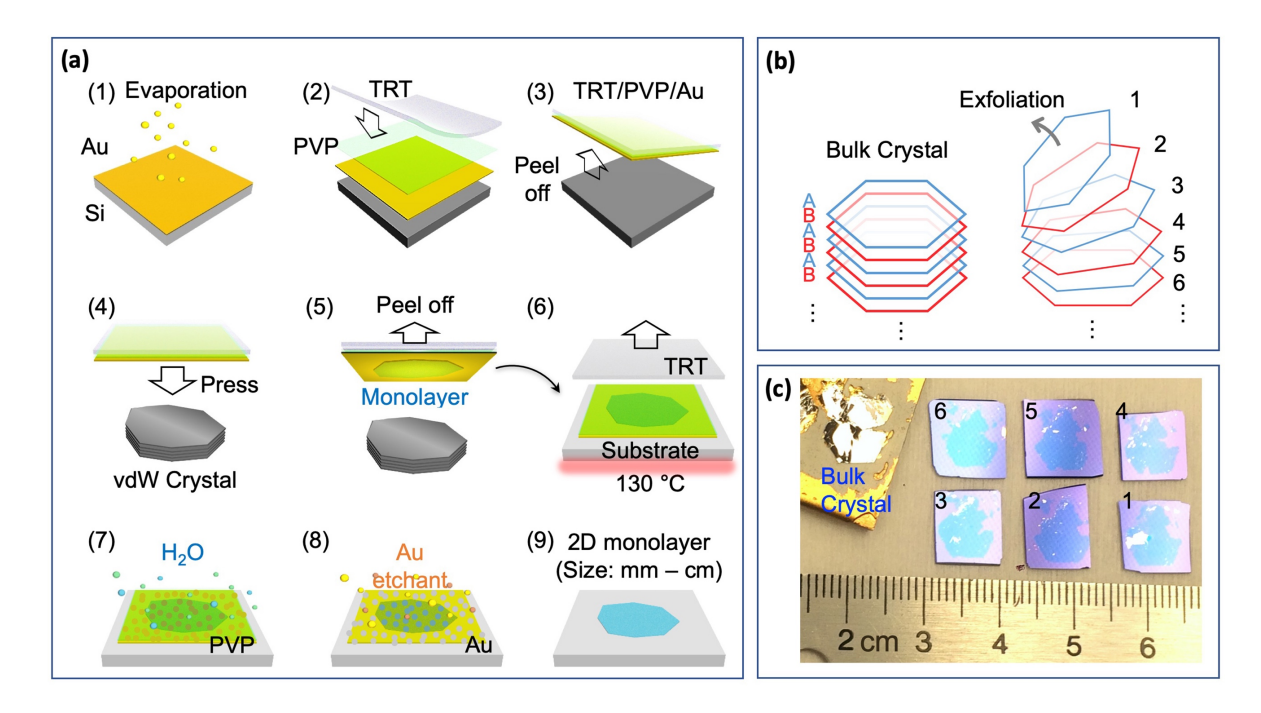


Figure 1. Schematics illustration of the layer-by-layer exfoliation procedure of bulk vdW single crystals. (a) The method: (1) Depositing gold on an ultra-flat silicon wafer; (2) Spin-coating the surface with a layer of PVP; (3) Using thermal release tape (TRT) to pick up the PVP/Au; (4) Pressing the ultra-flat gold onto the surface of a bulk vdW crystal; (5) Peeling off a monolayer and transferring onto a substrate; (6) Removing the thermal release tape with heat; (7) Dissolving PVP in water; (8) Dissolving gold in an I_2/I^- etchant solution; (9) The single crystal monolayer with macroscopic dimensions is obtained. (b) Schematics of the layer-by-layer exfoliation technique to yield even and odd layers from an AB-stacked vdW crystal. (c) Optical images of six monolayer samples (1-6, on SiO₂/Si substrate) sequentially exfoliated from a cm-size WSe₂ single crystal shown at the upper-left corner.

The strong adhesion of gold to TMDCs can repeatedly generate complete single crystal monolayers, each adopting the shape of the entire surface of a bulk crystal (Fig. 1b), as illustrated for six WSe₂ monolayers in Fig. 1c. The yield of exfoliation, expressed as the percentage of monolayer area picked up from the contacted bulk crystal surface, is close to unity. This technique can be applied to a broad range of vdW crystals, as we demonstrate here for single crystal TMDC monolayers (WS₂, MoS₂, WSe₂, MoSe₂, and ReS₂) on various substrates, such as SiO₂/Si, fused silica, and sapphire. Adhesion of the ultra-flat gold to graphene and hexagonal boron nitride (h-BN) is weaker, and the monolayers are smaller than for TMDCs, but still much larger than obtained

by conventional Scotch tape exfoliation. Optical images of the macroscopic TMDC monolayers are shown in Fig. S1. Each TMDC sample is dominated by the single crystal monolayer, sometimes with small regions of multilayers near the edges, resulting from the contact of the gold tape to imperfect or non-flat regions on the edges of TMDC bulk crystal.

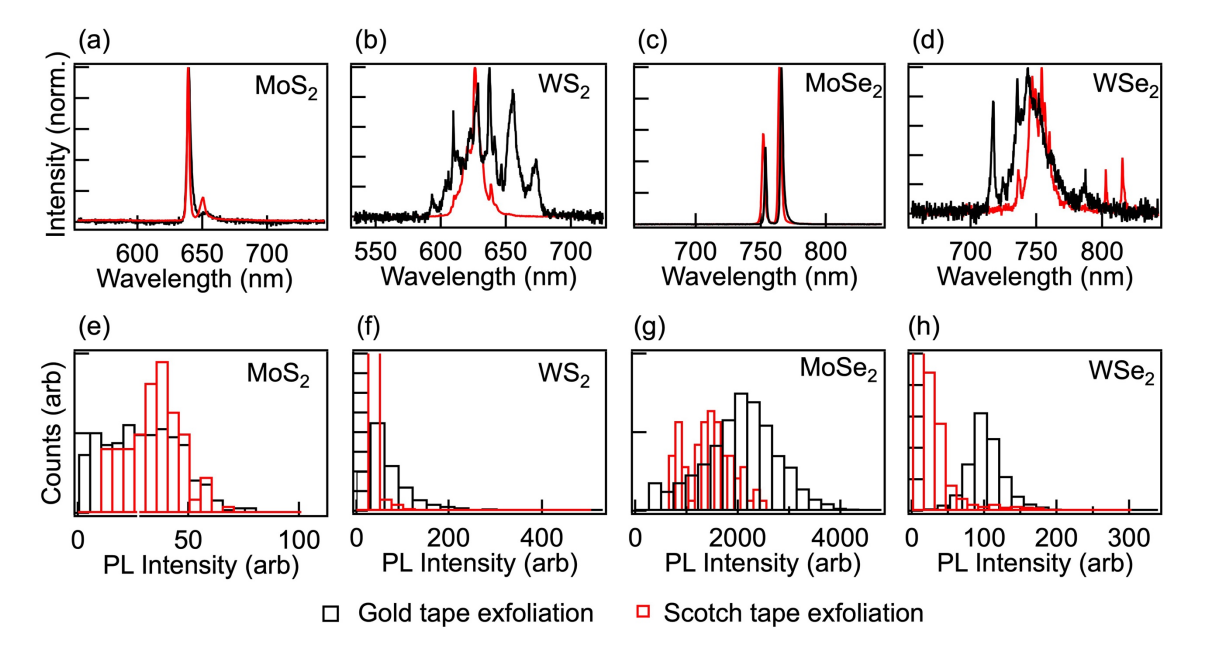


Figure 2. Comparison of PL spectra and intensity distributions in TMDC monolayers exfoliated from the gold tape (black) and Scotch tape (red) methods. PL spectra (top) and intensity distributions (bottom) for monolayers encapsulated in BN. Black: Gold tape exfoliated monolayers; Red: Traditional scotch tape exfoliated monolayers. MoSe₂ and WSe₂ monolayers from both methods are exfoliated from the same low-defect density bulk crystals grown from the flux-methods. The MoS₂ and WS₂ monolayers in both methods are exfoliated from the same chemical vapor transport grown bulk crystals. All PL measurements were at 4 K on monolayer samples with BN encapsulation.

The quality of the large single crystal monolayer is comparable to or slightly better than that of microscopic single crystal monolayers produced from traditional Scotch tape method, as evidenced in the clean surface characterized by atomic force microscopy (AFM) and the crystal quality characterized by photoluminescence (PL) spectroscopy. AFM image of the TMD monolayer flakes reveals atomic scale flatness, as shown in Fig. S2 for a MoS2 monolayer. PL spectroscopy is particularly sensitive to defects and disorder, as increased peak width is evidence of inhomogeneous broadening (disorder) and reduced intensity indicative of defect-mediated nonradiative recombination. We compare in Fig. 2 low temperature PL spectra of the macroscopic TMDC monolayers from our gold tape method and microscopic monolayers from the commonly used Scotch tape method, with all monolayers encapsulated in h-BN to eliminate the effect from

substrate defects and inhomogeneity. The MoSe₂ and WSe₂ crystals are from flux-growth,(22) MoS₂ from natural crystals (SPI Supplies), and WSe₂ from chemical vapor transport growth (HQ Graphene). Note that the highest quality MoSe₂ and WSe₂ crystals from flux-growth(22) are all of small sizes ($\sim 100 \, \mu m$) and we find that defect density in macroscopic sized crystals ($\geq 1 \, mm$) from flux growth typically is higher than those in the smaller sizes. For MoS₂ and MoSe₂, the PL spectra from the two methods are nearly identical. The former is characterized by the dominant A exciton and the latter shows the A exciton and the trion peaks, both nearly independent of the two exfoliation methods. PL image histogram analysis (Fig. 2) shows that the PL intensities from our macroscopic monolayers are consistent with or slightly higher than those from the Scotch tape method. For WS₂ and WSe₂ monolayers, the PL spectra from methods are similarly complex due to the presence of dark excitons and many-body states;(23, 24) however overall PL intensity in our macroscopic monolayers is still comparable to or slightly higher than those from the Scotch tape method. These results confirm the high quality of the macroscopic TMDC monolayers.

Obtaining macroscopic single crystal monolayers of 2D vdW crystals with high throughput opens the door to a broad range of applications, spanning from spectroscopy, to scalable devices, and to the easy assembly of artificial lattices. For example, the macroscopic size of the TMDC monolayers prepared on transparent substrates allows us to use a conventional UV-Vis

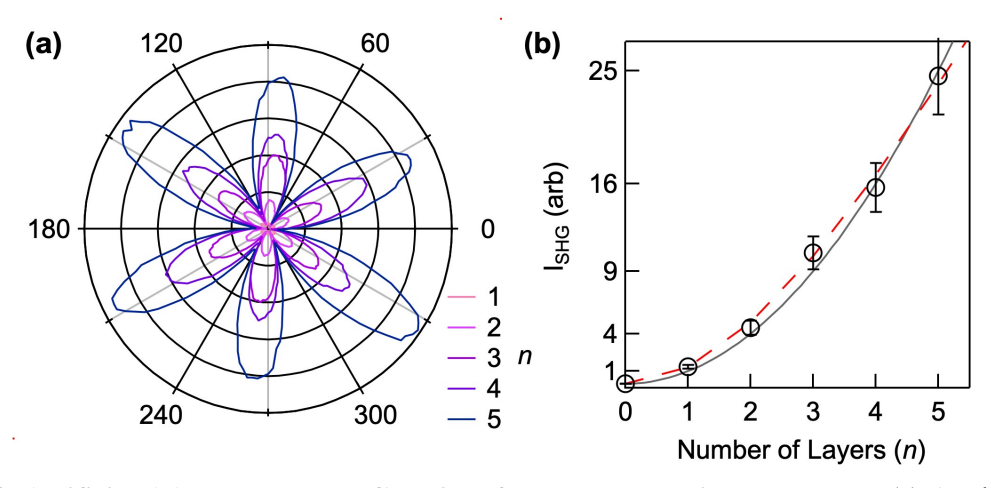


Figure 3. Artificial AA stacked TMDC lattices from macroscopic monolayers. (a) Angle-resolved SHG intensity of AA stacked MoSe₂ artificial lattices as a function of the rotation angle of crystal with respect to light polarization. (b) Integrated SHG intensity (circles) for different number of layers in the AA stacks. The solid line is a quadratic fit, while the red dashed line is fit which takes into account of both coherent interference and re-absorption, as discussed in the supplementary information. We fabricate each multilayer sample by picking up the monolayers on SiO₂ substrates sequentially with the ultra-flat gold tape, with SHG measurement carried out on the gold tape after each step.

spectrometer to easily obtain optical absorption spectra of TMDC monolayers (Fig. S3), each featuring the well-known A and B excitons.(25) More importantly, the effective disassembly of the bulk crystal into individual single crystal monolayers with defined crystal orientation allows us to reassemble them into artificial vdW crystals with desired properties. Specifically, we show that the ultra-flat gold tape can be used as an effective pick-up tool to reassemble higher-order vdW lattices from the macroscopic single crystals. We demonstrate two examples: (1) the reassembly of macroscopic TMDC monolayers into an artificial crystal lattice with AA stacking for greatly enhanced nonlinear optical response; and (2) the formation of a macroscopic heterobilayer from two distinct TMDC monolayers.

The first example targets effective engineering of nonlinear optical properties in an ultrathin material. TMDC monolayers, with intrinsically broken inversion symmetry, are known to possess ultra-strong nonlinear susceptibilities as reflected in intense second harmonic generation (SHG).(26–28) However, TMDC bulk crystals exhibit 2H centro-symmetry; the crystal orientation of neighboring layers are 180° counter-aligned with each other in the so-called AB stacking. Due to cancellation between counter-aligned layers, the SHG response is smaller in few-layer samples, becoming asymptotically negligible for the bulk crystal. (26–28) Indeed, interference in SHG from individual monolayers in stacked homo- or hetero-bilayers is very sensitive to the alignment angle between the two layers. (29) We disassemble TMDC bulk crystal into individual monolayers and reassemble the even (or odd) monolayers into AA artificial crystals. Figure 3a shows angleresolved SHG responses from 1-5 layers of an AA-stacked MoSe₂ artificial lattice, with the integrated SHG intensities (I_{SHG} , circles) plotted against the number (n) of the monolayers in Fig. 3b. Similar results for AA stacked MoS2 are shown in Fig. S4. The dashed line in Fig. 3b corresponds to fit which takes into account re-absorption and interference of SHG from different layers. At ultrathin thickness, the SHG response is dominated by constructive interference from adjacent layers, close to the ideal limit of a quadratic optical response, $I_{SHG} \propto n^2$, the solid curve in Fig. 3b. The close to perfect coherent enhancement benefits from the negligible phase mismatch over nanometer distances. With increasing thickness of the artificial lattice, the increase of coherent response is expected to continue, until 10s nm when phase mismatch and reabsorption of SHG light become significant, as is shown in Fig. S5. While synthesis of 3R phases of TMDC with broken inversion symmetry is possible, (30) our method is unrestricted by synthesis and can be used to construct any macroscopic vdW multilayer structures with control in interlayer twist

angles and chemical identities. As one indication of the consistency of the artificial lattices from our macroscopic monolayers, we measure SHG responses from the $MoSe_2/WSe_2$ at five randomly picked spots, Fig. S6. The orientation of the artificial lattice is unchanged from spot-to-spot within the experimental angular resolution of $\pm 0.5^{\circ}$. The SHG intensity variation is within $\pm 15\%$, which is likely due to small changes in optical alignment as the sample is moved macroscopically under the microscope.

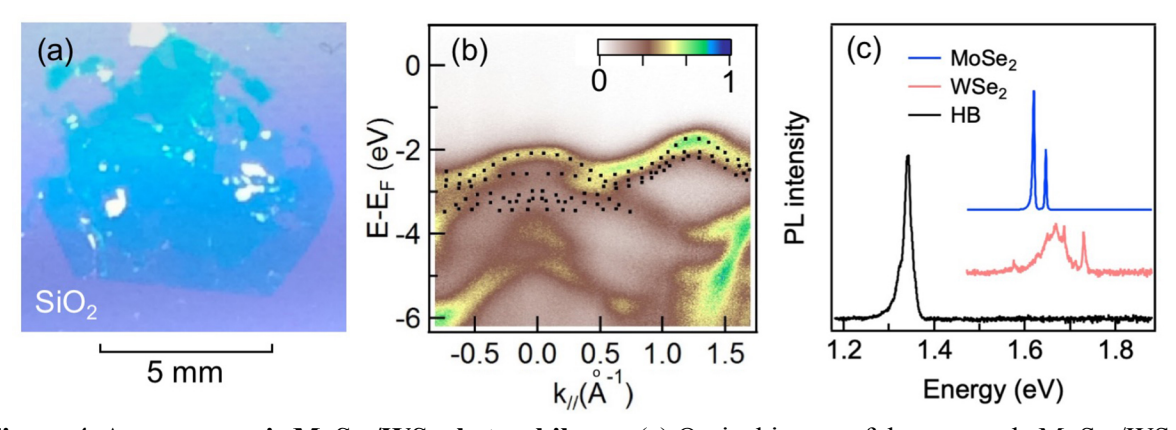


Figure 4. A macroscopic MoSe₂/WSe₂ heterobilayer. (a) Optical image of the mm scale MoSe₂/WSe₂ heterostructure on SiO₂/Si substrate aligned at $\Delta\theta$ = 3.0±0.5°, as determined in SHG; (b) Angle-resolved photoemission spectrum (ARPES) of the mm scale MoSe₂/WSe₂ heterobilayer measured along Γ - K direction. The dotted curves are theoretical calculations from ref. (*31*). The sample was at 295 K in ARPES measurement; (c) Low temperature (4K) PL spectra of interlayer exciton in h-BN encapsulated MoSe₂/WSe₂ heterobilayer (HB, black). For comparison, we also show PL spectra from intralayer excitons in h-BN encapsulated MoSe₂ (blue) and WSe₂ (red) monolayers. All monolayers were exfoliated with the gold tape method. For the macroscopic heterobilayer on oxide-terminated silicon in (a) and (b), we used commercial CVT grown MoSe₂ and WSe₂ crystals. For the h-BN encapsulated samples in (c), we used higher quality but smaller flux-grown MoSe₂ and WSe₂ crystals.

The second example is the creation of heterobilayers with controlled twist angle from two macroscopic single crystal monolayers. By precisely engineering angular and/or lattice mismatch, vdW bilayers constructed from the same or different single crystal 2D monolayers have been shown to exhibit a range of quantum phenomena, but all on μ m scale samples form the Scotch tape method.(4–12) An intriguing development for their future technological applications is generation of such bilayer structures at macroscopic dimensions. Using two monolayers of MoSe₂ and WSe₂, we fabricated a MoSe₂/WSe₂ single crystal heterobilayer, as is shown in optical image in Fig. 4a, with lateral dimensions of ~4 mm and with twist angle of $\Delta\theta$ =3.0±0.5°. AFM imaging on part of the macroscopic structure identifies the heterobilayer with a high degree of flatness (Fig. S7). The

large size of the single crystal heterobilayer on a dielectric substrate (SiO₂) allows us to map out the band structure using angle resolved photoemission spectroscopy (ARPES) using a conventional setup with hemispherical electron energy analyzer, without microscopic capabilities. The ARPES spectrum determined in the Γ-K direction is in excellent agreement with theoretical calculations (Fig. 4b).(31) Low temperature PL measurement of BN encapsulated heterobilayer stack reveals the dominant radiative recombination from the charge separated interlayer exciton (Fig. 4c), in excellent agreement with previous reports of interlayer excitons in MoSe₂/WSe₂ heterobilayers fabricated from the Scotch-tape method.(32–34) Moreover, the intralayer excitons from constituent monolayers in our heterobilayer sample are completely quenched, verifying the high quality of the MoSe₂/WSe₂ interface. Note that the detailed peak shape and intensity of interlayer exciton PL vary from location-to-location on the sample (Fig. S8-S10), which is well known in recent reports on the same system(8, 9) and is a likely result of sensitivity of PL emission to local variation in electrostatic environment and strain.(35)

To summarize, we show a general method for the facile disassembly of vdW single crystals layer-by-layer into monolayers with macroscopic dimensions. The quality of the macroscopic single crystal monolayers are comparable to those of microscopic dimensions obtained from the state-of-the-art Scotch-tape method, as confirmed in AFM imaging and PL characterization. We demonstrate this method for the controlled re-assembly of these macroscopic monolayers into artificial lattices, including AA stacked TMDC multilayers for dramatically enhanced nonlinear optical response and heterobilayers for interlayer exciton at macroscopic dimensions. This approach may allow us to extend the exciting discoveries in the so-called "twistronics", i.e., magicangle or moiré landscapes in 2D bilayers,(4–12) into the multilayer or bulk region. The latter is a formidable challenge for microscopic monolayers from the Scotch-tape method, but achievable with our macroscopic monolayers. With techniques for the high-throughput production of macroscopic monolayers, 2D quantum devices on a large scale may become a reality.

References

- 1. K. S. Novoselov *et al.*, Electric Field Effect In Atomically Thin Carbon Films. *Science*. **306**, 666–669 (2004).
- 2. K. S. Novoselov, A. Mishchenko, A. Carvalho, A. H. C. Neto, 2D Materials And van der Waals Heterostructures. *Science*. **353**, aac9439 (2016).

- 3. H. Y. Yu *et al.*, Moire Excitons: From Programmable Quantum Emitter Arrays To Spin-Orbit-Coupled Artificial Lattices. *Sci. Adv.* **3**, e1701696 (2017).
- 4. Y. Cao *et al.*, Unconventional Superconductivity in Magic-Angle Graphene Superlattices. *Nature.* **556**, 43–50 (2018).
- 5. Y. Cao *et al.*, Correlated Insulator Behaviour at Half-Filling in Magic-Angle Graphene Superlattices. *Nature.* **556**, 80–84 (2018).
- 6. C. Jin *et al.*, Observation of Moiré Excitons in WSe₂/WS₂ Heterostructure Superlattices. *Nature*. **567**, 76–80 (2019).
- 7. E. M. Alexeev *et al.*, Resonantly Hybridized Excitons in Moiré Superlattices in van der Waals Heterostructures. *Nature*. **567**, 81–86 (2019).
- 8. K. L. Seyler *et al.*, Signatures of Moiré-Trapped Valley Excitons in MoSe₂/WSe₂ Heterobilayers. *Nature*. **567**, 66–70 (2019).
- 9. K. Tran *et al.*, Evidence for Moiré Excitons in Van Der Waals Heterostructures. *Nature*. **567**, 71–75 (2019).
- 10. Q. Tong *et al.*, Topological Mosaics in Moiré Superlattices of van der Waals Heterobilayers. *Nat. Phys.* **13**, 356–362 (2017).
- 11. L. Wang *et al.*, Magic Continuum in Twisted Bilayer WSe₂. *arXiv Prepr. arXiv1910.12147* (2019).
- 12. X. Lu *et al.*, Superconductors, Orbital Magnets and Correlated States in Magic-Angle Bilayer Graphene. *Nature.* **574**, 653–657 (2019).
- 13. J. N. Coleman *et al.*, Two-Dimensional Nanosheets Produced by Liquid Exfoliation of Layered Materials. *Science.* **331**, 568–571 (2011).
- 14. Z. Cai, B. Liu, X. Zou, H.-M. Cheng, Chemical Vapor Deposition Growth and Applications of Two-Dimensional Materials and Their Heterostructures. *Chem. Rev.* **118**, 6091–6133 (2018).
- 15. G. Z. Magda *et al.*, Exfoliation of Large-Area Transition Metal Chalcogenide Single Layers. *Sci. Rep.* **5**, 14714 (2015).
- 16. M. Velický *et al.*, Mechanism of Gold-Assisted Exfoliation of Centimeter-Sized Transition-Metal Dichalcogenide Monolayers. *ACS Nano.* **12**, 10463–10472 (2018).
- 17. S. B. Desai *et al.*, Gold-Mediated Exfoliation of Ultralarge Optoelectronically-Perfect Monolayers. *Adv. Mater.* **28**, 4053–4058 (2016).
- 18. J. Shim *et al.*, Controlled Crack Propagation for Atomic Precision Handling of Wafer-Scale Two-Dimensional Materials. *Science*. **362**, 665–670 (2018).
- 19. Y. Liu *et al.*, Approaching the Schottky–Mott Limit in van der Waals Metal–Semiconductor Junctions. *Nature*. **557**, 696–700 (2018).
- 20. M. Hegner, P. Wagner, G. Semenza, Ultralarge Atomically Flat Template-Stripped Au Surfaces for Scanning Probe Microscopy. *Surf. Sci.* **291**, 39–46 (1993).

- 21. N. Vogel, J. Zieleniecki, I. Köper, As Flat As It Gets: Ultrasmooth Surfaces From Template-Stripping Procedures. *Nanoscale*. **4**, 3820–3832 (2012).
- 22. D. Edelberg *et al.*, Approaching the Intrinsic Limit in Transition Metal Diselenides via Point Defect Control. *Nano Lett.* **19**, 4371–4379 (2019).
- 23. Y. You et al., Observation of Biexcitons in Monolayer WSe₂. Nat. Phys. 11, 477 (2015).
- 24. G. Plechinger *et al.*, Identification of Excitons, Trions and Biexcitons in Single-Layer WS₂. *Phys. status solidi Rapid Res. Lett.* **9**, 457–461 (2015).
- 25. Y. Li *et al.*, Measurement of the Optical Dielectric Function of Monolayer Transition-Metal Dichalcogenides: MoS₂, MoSe₂, WS₂, and WSe₂. *Phys. Rev. B.* **90**, 205422 (2014).
- 26. Y. Li *et al.*, Probing Symmetry Properties of Few-Layer MoS₂ and h-BN by Optical Second-Harmonic Generation. *Nano Lett.* **13**, 3329–3333 (2013).
- 27. C. Janisch *et al.*, Extraordinary Second Harmonic Generation in Tungsten Disulfide Monolayers. *Sci. Rep.* **4**, 5530 (2014).
- 28. A. Säynätjoki *et al.*, Ultra-Strong Nonlinear Optical Processes and Trigonal Warping in MoS₂ Layers. *Nat. Commun.* **8**, 893 (2017).
- 29. W. Hsu *et al.*, Second Harmonic Generation from Artificially Stacked Transition Metal. *ACS Nano.* **8**, 2951–2958 (2014).
- 30. J. Shi *et al.*, 3R MoS₂ with Broken Inversion Symmetry: A Promising Ultrathin Nonlinear Optical Device. *Adv. Mater.* **29**, 1701486 (2017).
- 31. R. Gillen, J. Maultzsch, Interlayer Excitons in MoSe₂WSe₂ Heterostructures From First Principles. *Phys. Rev. B.* **97**, 165306 (2018).
- 32. P. Rivera *et al.*, Observation of Long-Lived Interlayer Excitons in Monolayer MoSe₂– WSe₂ Heterostructures. *Nat. Commun.* **6**, 6242 (2015).
- 33. P. Rivera *et al.*, Valley-Polarized Exciton Dynamics in A 2D Semiconductor Heterostructure. *Science*. **351**, 688–691 (2016).
- 34. J. Wang *et al.*, Optical Generation of High Carrier Densities in 2D Semiconductor Heterobilayers. *Sci. Adv.* **5**, eaax0145 (2019).
- 35. Y. Bai *et al.*, One-Dimensional Moiré Excitons in Transition-Metal Dichalcogenide Heterobilayers. *arXiv Prepr. arXiv1912.06628* (2019).
- 36. D. Rhodes, S. H. Chae, R. Ribeiro-Palau, J. Hone, Disorder In van der Waals Heterostructures of 2D Materials. *Nat. Mater.* 18, 541–549 (2019).
- 37. C. Hsu, R. Frisenda, R. Schmidt, A. Arora, S. M. de Vasconcellos *et al.*, Thickness-Dependent Refractive Index of 1L, 2L, and 3L MoS₂, MoSe₂, WS₂, and WSe₂. *Adv. Opt. Mater.* 7, 1900239 (2019).

38. O. A. Ajayi, J. V Ardelean, G. D. Shepard, J. Wang, A. Antony *et al.*, Approaching The Intrinsic Photoluminescence Linewidth in Transition Metal Dichalcogenide Monolayers. *2D Mater.* **4**, 31011 (2017).

Acknowledgements

Funding: The development of ultra-flat gold tape exfoliation method was supported by the Center for Precision Assembly of Superstratic and Superatomic Solids, a Materials Science and Engineering Research Center (MRSEC) through NSF grant DMR-1420634. All TMDC sample preparation, imaging, and spectroscopy experiments were supported by the National Science Foundation (NSF) grant DMR-1809680. XYZ acknowledges support by the Vannevar Bush Faculty Fellowship through Office of Naval Research Grant # N00014-18-1-2080 for the purchase of the laser system used in the ARPES measurements. FL acknowledges support by the Department of Energy (DOE) Office of Energy Efficiency and Renewable Energy (EERE) Postdoctoral Research Award under the EERE Solar Energy Technologies Office administered by the Oak Ridge Institute for Science and Education (ORISE). ORISE is managed by Oak Ridge Associated Universities (ORAU) under DOE contract number DE-SC00014664. All opinions expressed in this paper are the author's and do not necessarily reflect the policies and views of DOE, ORAU, or ORISE.

Author contributions:

X.-Y.Z. and F.L. conceived this work. F.L. performed all experiments on gold-tape exfoliation and characterization. W.W performed experiments on scotch tape exfoliation and BN encapsulation. Y.B. and F.L. measured the low temperature PL. J.H. and S.H.C conceived the idea of using PVP protection layer. Q.L. assisted with gold-tape exfoliation and SHG measurement. J.W. and Y.B. constructed the low temperature PL mapping setup. F.L. and X.-Y.Z. wrote the manuscript with inputs from all coauthors. X.-Y.Z. supervised the project. All authors participated in the discussion and interpretation of the results.

Competing interests: Part of this work is included in a US provisional patent application.

Data and materials availability: All data needed to evaluate the conclusions in the paper are present in the paper or the Supplementary Materials.

Supplementary Materials

Materials and Methods

Fig S1 to S10

References (36-38)

SUPPLEMENTARY INFORMATION

Disassembling 2D van der Waals Crystals into Macroscopic Monolayers and Reassembling into Artificial Lattices

Fang Liu¹, Wenjing Wu¹, Yusong Bai¹, Sang Hoon Chae², Qiuyang Li¹, Jue Wang¹, James Hone², X.-Y. Zhu^{1,*}

References (36-38)

MATERIALS AND METHODS

The gold tape exfoliation

A 150 nm thickness gold layer is deposited onto flat silicon substrate (NOVA Electronic Materials LLC, p type doped) with e-beam evaporation (Angstrom Engineering EvoVac Multi-Process thin film deposition system). A layer of polyvinylpyrrolidone (PVP) solution (Sigma Aldrich, mw 40000, 10% wt in ethanol/acetonitrile wt 1/1) is spin-coated on the top of the Au film (3000 rpm, acceleration 1000rpm/s, 2min) and cured at 150 °C for 5 min as a sacrificial layer to prevent tape residue contamination. The prepared PVP/Au is picked up with thermal release tape (semiconductor corp. release temperature 90 °C), revealing an ultra-flat, clean, and fresh gold surface, i.e., the gold tape. The gold tape is gently pressed onto a freshly cleaved bulk vdW crystal, including a MoS₂ natural single crystal (SPI Supplies), WS₂, MoSe₂, WSe₂, and ReS₂ single crystals (HQ graphene), and the MoSe₂ and WSe₂ single crystals from a flux-growth method with significantly reduced defect density. (36) As the tape is lifted off the surface, it carries the PVP/Au layer with a monolayer 2D crystal attached to Au surface, and is further transferred onto the desired substrate. The thermal release tape is removed by heating at 130 °C. The PVP layer is removed by dissolving in deionized (DI) water for 2 h. The sample on the substrate covered by Au is rinsed

¹ Department of Chemistry, Columbia University, New York, NY 10027, USA

² Department of Mechanical Engineering, Columbia University, New York, NY 10027, USA

^{*} To whom correspondence should be addressed. Email: xyzhu@columbia.edu

with acetone and cleaned by O_2 plasma for 3 min to remove any remaining polymer residues. The Au layer is dissolved in a KI/I₂ gold etchant solution (2.5g I₂ amd 10g KI in 100ml DI water. Iodine, 99.99%, Alfa Aesar; potassium iodide, 99.9%, Alfa Aesar). The monolayer is rinsed with DI water and isopropanol, and dried with N₂. For stacking of multiple AA stacks, a collection of single crystal monolayers from the same single crystal is prepared on SiO₂/Si substrates (SiO₂ thickness = 285 nm) with known sequences of odd-even order. An ultra-flat gold tape, freshly peeled off the Si templating surface, is used to pick up only even or odd monolayers sequentially with angular alignment, $\Delta\theta = 0.0\pm0.5^{\circ}$. The SHG measurements are performed on the stacked monolayers on Au after each pick up. For stacking of macroscopic heterobilayer, a freshly prepared gold tape is used to pick up a MoSe₂ monolayer and then pressed onto another freshly prepared WSe₂ monolayer on the SiO₂/Si substrate with pre-determined alignment angle, followed by the same rinsing and etching procedure.

BN encapsulation

Thin BN flakes for encapsulation are exfoliated with scotch tape onto the SiO₂/Si surface (SiO₂ thickness 285nm). The TMDC monolayers are prepared either from our gold tape technique or traditional scotch tape exfoliation onto the SiO₂/Si substrate. A film of poly-propylene carbonate (PPC) are prepared on top of a small polydimenthylsiloxane (PDMS) stamp taped on a glass slide. The glass slide is inverted and fixed on a transfer stage with objective lens, and is used to sequentially pick up the flakes with controlled contact point. Lifting of the first BN flake is achieved by controlled expansion of PPC through increasing and decreasing temperature near 40 °C. After the first BN flake is picked up to PPC, the process is repeated to pick up the TMD monolayer and the last layer of BN. The thin flakes are more adhesive to BN than to SiO₂/Si substrate, permitting encapsulation of BN/TMD/BN stacks on PPC surface. The stack is further transferred onto desired substrate by heating substrate to 90-120°C to melt PPC and pushing the PPC onto the substrate, allowing the stack to stay on the substrate while the glass slide and PDMS are removed.

Material characterizations

The SHG measurements are performed at room temperature on an inverted microscope (Olympus IX73, with 100x objective). The pump 800 nm for SHG is generated from an ultrafast Ti:Sapphire oscillator (SpectraPhysics Tsunami, pumped by Sprout D, 5W, Lighthouse Photonics),

and reflected off a 650 nm short-pass dichroic mirror, and is focused onto the sample with a 100x objective. The SHG of the sample transmits through the 650nm short-pass dichroic mirror and a 400nm bandpass filter before it is collected with a photomultiplier tube. The signal is amplified and detected with a photon counter. The polarization for both the input laser and the collection path are rotated simultaneously relative to the sample, by rotating a half waveplate between the objective and the dichroic mirror, intersecting both the excitation and collection path. Therefore, the polarization response of SHG is equal to rotating the sample, giving rise to a 6-fold symmetry.

For ARPES measurements, the TMDC heterostructure on SiO₂/Si substrate is transferred to an ultrahigh vacuum chamber (~10⁻¹⁰ Torr) and annealed at 200 °C for 4 h via direct current heating to remove residual contaminants. A gold contact is placed on the side for grounding. The ARPES measurements are carried out in the ultrahigh vacuum at room temperature. For photoionization, a 22 eV extreme UV radiation is obtained from high harmonic generation (HHG) from 400 nm input laser light in Kr gas. The 400 nm light comes from the second harmonic of the output of a regenerative Ti:Sapphire amplifier (Coherent Legend Elite Duo HE+, 10 kHz, 35 fs). HHG is generated in a modified KMLabs XUUS4 high harmonics system. The kinetic energy of the photoemitted electrons are measured on a hemispherical electron energy analyzer equipped with a 2D delay line detector (SPECS Phoibos-100).

Confocal microscopy PL imaging

The TMDC heterobilayer and monolayer samples on SiO₂/Si substrates are placed in a liquid helium recirculating optical cryostat (Montana Instruments Fusion/X-Plane) at 4 K in vacuum (<10⁻⁶ torr). The incident laser beam (532 nm, CW) is focused on the sample by a 100x, NA 0.75 objective (Zeiss LD EC Epiplan-Neofluar 100x/0.75 HD DIC M27) to a diffraction limited spot. The excitation power is approximately 80 μW, measured by a calibrated power meter (Ophir StarLite). PL emissions from the sample plane are imaged with a home-built scanning confocal microscope system with a Galvo-Galvo scanner (Thorlabs, GVS012/M). The photoluminescence is collected by the same objective, focused into a spectrograph (Princeton Instruments, IsoPlane 160) and detected by a liquid-N₂ cooled InGaAs photodiode array (Princeton Instruments PyLoN-IR) within the desired wavelengths.

Simulation of second harmonic generation

The wave propagation of 400 nm and 800 nm light in the SHG process is calculated with the reported optical constants, (25,37) taking into the account a) absorption of 400 nm and 800 nm as they propagate through the thin layer crystal and b) interference of 400 nm generated from each layer. The simulated results are displayed in Figure S5. The red curve shows the quadratic response for coherent interference enhancement assuming zero phase delay/reabsorption for SHG from all layers. At few layer numbers, the simulation is close to the quadratic response. With increasing thickness of the AA stacked lattice, phase mismatch and reabsorption of SHG light become significant, and the response deviates from quadratic coherent enhancement. The peak of the enhancement is predicted to be approximately 60 fold for MoS₂ AA stacked layers, which is consistent with the highest SHG enhancement reported from different thickness of 3R phase MoS₂, which is non-centrosymmetric with AA stack interlayer alignment. (30)

ADDITIONAL RESULTS

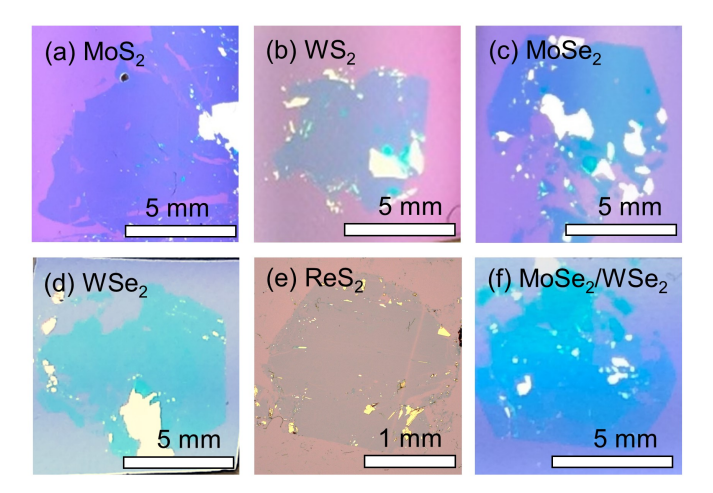


Figure S1. Optical images of 2D single crystals. TMDC monolayers, MoS₂, WS₂, MoSe₂, WSe₂, ReS₂ and heterobilayer, MoSe₂/WSe₂, are obtained from the method in Fig. 1. All 2D crystals in the image are on 285 nm SiO₂/Si substrates. Images taken with an iPhone camera.

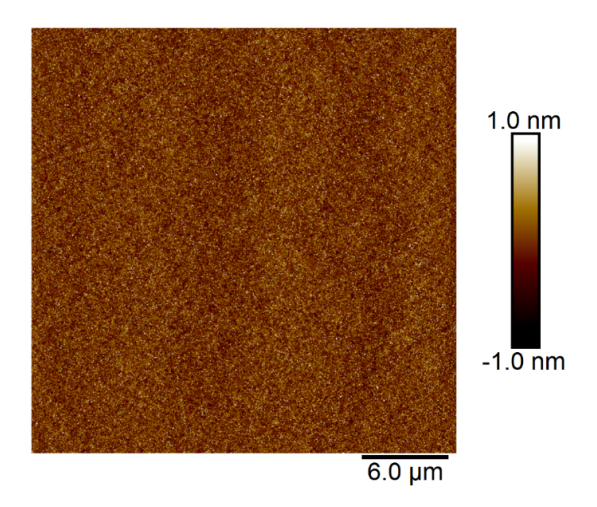


Figure S2. AFM image of a MoS₂ monolayer on a SiO₂/Si substrate. The monolayer from the gold tape exfoliation method shows cleanness of the surface over a large area. AFM measurements are performed on a Bruker Dimension Fastscan AFM.

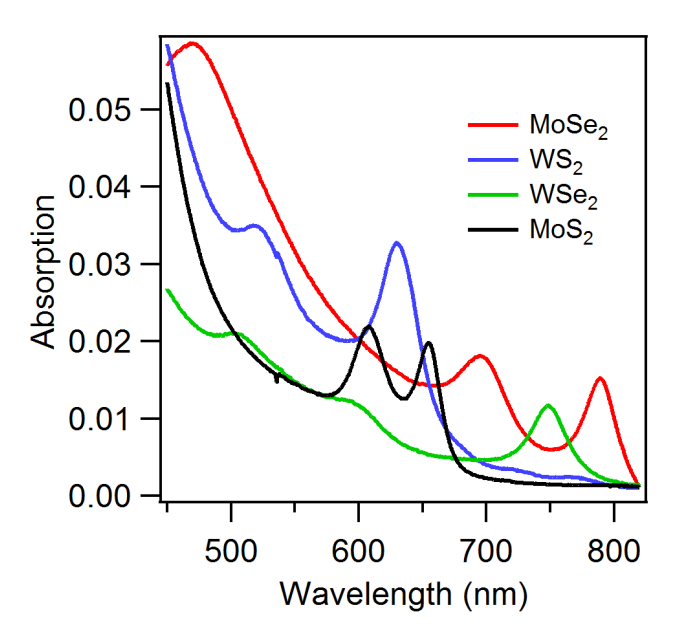


Figure S3. UV-Vis spectra of the macroscopic monolayers prepared from the gold tape exfoliation on fused silica substrates. The UV-Vis is measured at room temperature with a commercial UV-Vis spectrometer (UV-1800, Shimadzu Corp.). The spectra are displaced for clarity.

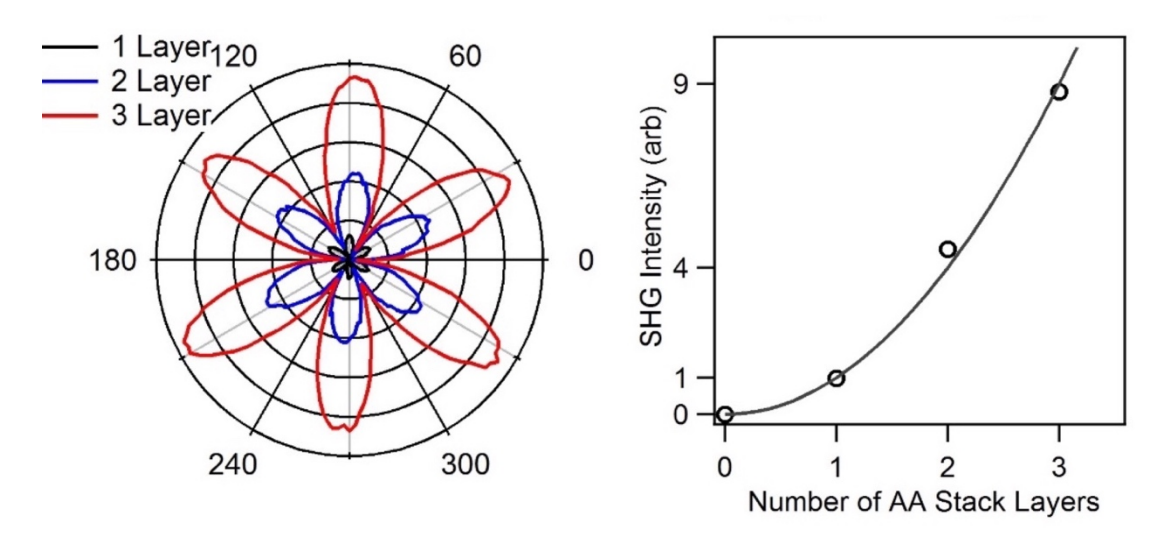


Figure S4. SHG from AA stacked macroscopic single crystal multilayers of MoS₂. Left: SHG angular distributions of 1, 2, and 3 layers; Right: integrated SHG intensity (circles) as a function of the number (n) of AA-stacked MoS₂ multilayers. Solid curve shows a quadratic function (n^2) .

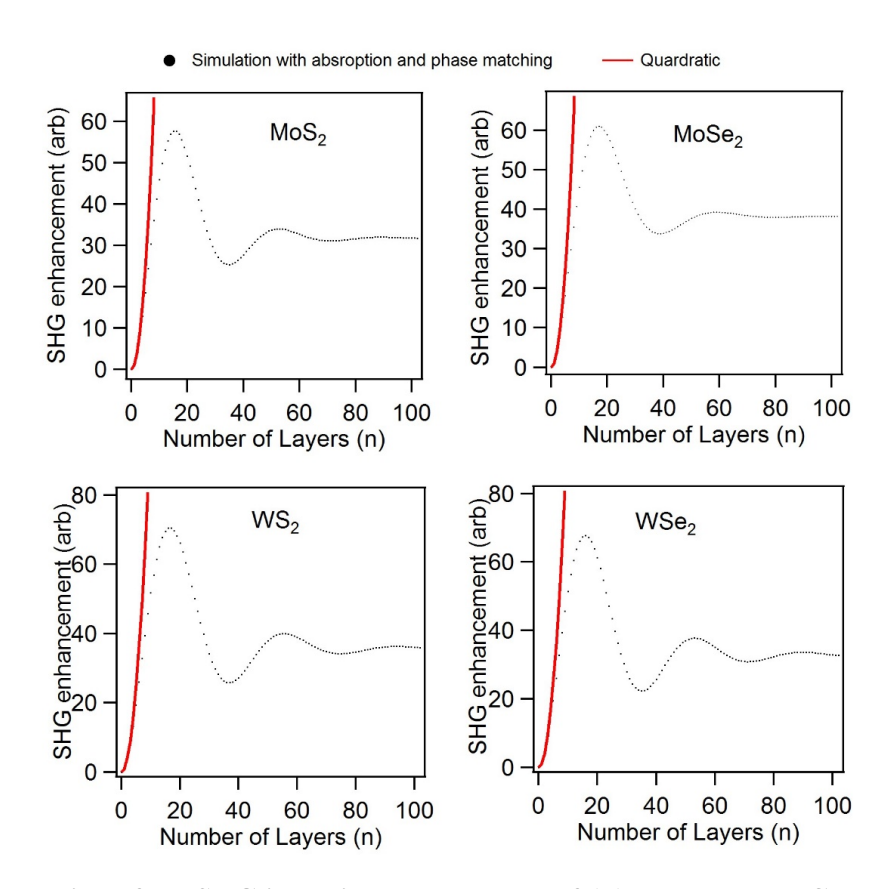


Figure S5. Simulation of the SHG intensity enhancement of AA stacked TMDC multilayers. The red line is quadratic, assuming no phase delay or reabsorption; the dotted line is simulation of the SHG intensity based on both real and imaginary refractive indices of TMDC bulk crystals.

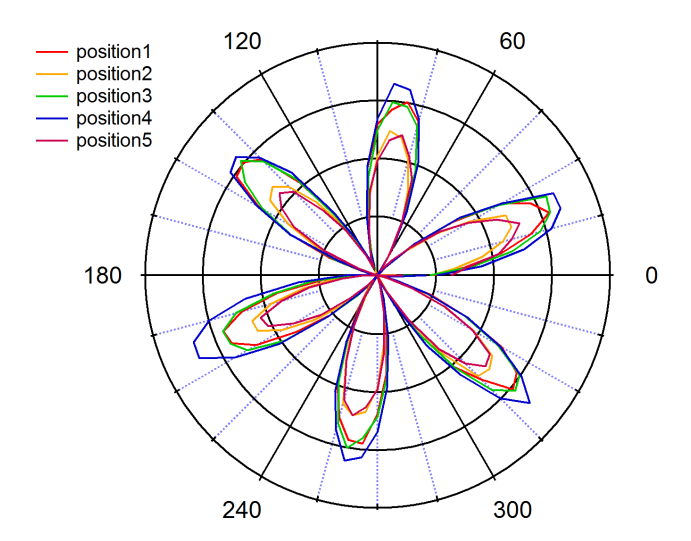


Figure S6. Angle-resolved SHG intensity of the $MoSe_2/WSe_2$ heterobilayer as a function of the rotation angle of crystal with respect to light polarization. This is the same sample as shown in Fig 4. The five colors represent data obtained from five randomly picked spots on the macroscopic sample. The variation in SHG intensity from spot to spot is approximately $\pm 15\%$ and this variation likely result from small changes in optical alignment as the sample is moved under the optical microscope. Most importantly, the alignment angles from spot-to-spot are unchanged within the experimental angular resolution of $\pm 0.5^{\circ}$.

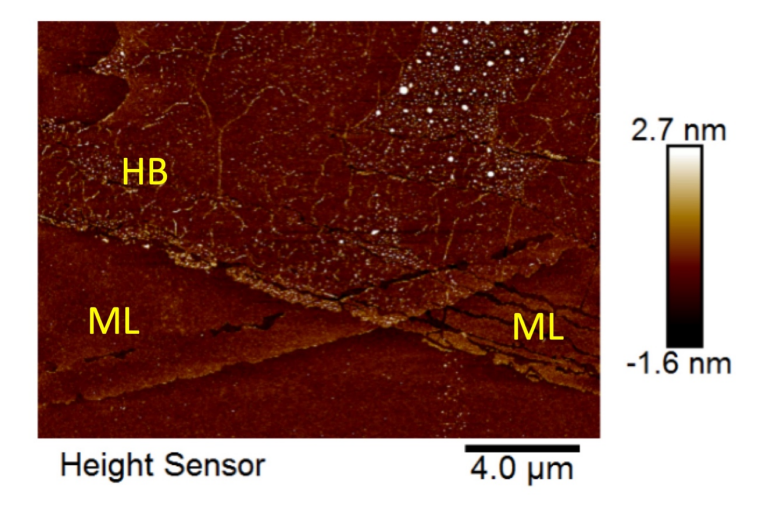


Figure S7. AFM image taken near the edge of the macroscopic MoSe₂/WSe₂ heterobilayer sample prepared by the gold tape exfoliation method on a SiO₂/Si substrate. The monolayer (ML) and heterobilayer (HB) regions are indicated. AFM measurements are performed on a Bruker Dimension Fastscan AFM.

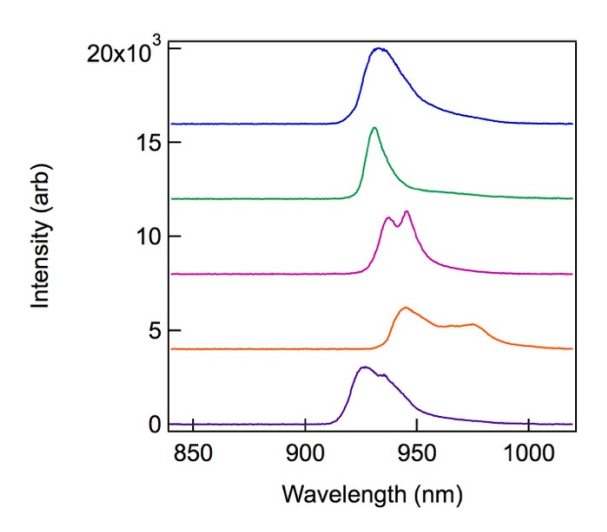


Figure S8. Low temperature (4K) PL spectra of interlayer exciton in h-BN encapsulated MoSe₂/WSe₂ heterobilayer. The five spectra (offset for clarify) are from five different locations. The sample was fabricated by the gold tape exfoliation method from flux-grown MoSe₂ and WSe₂ crystals.

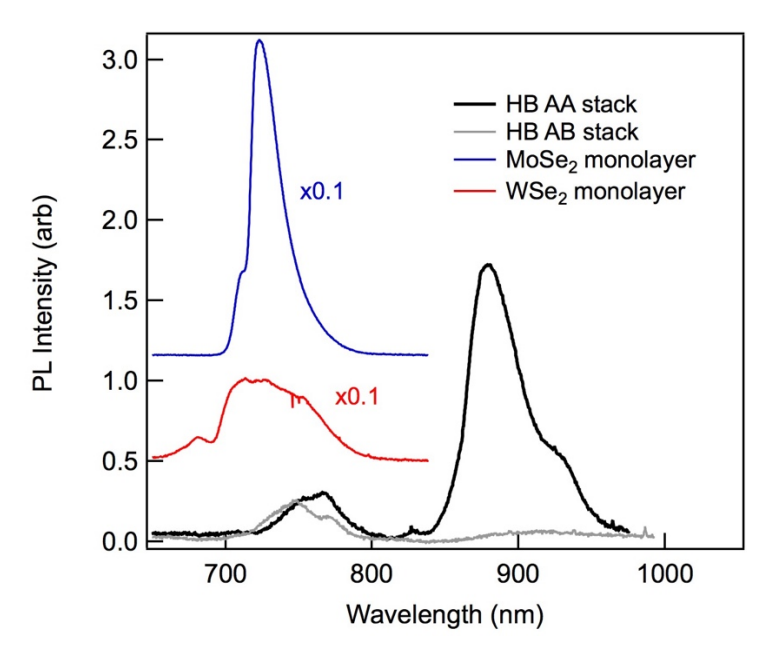


Figure S9. Low temperature (4K) PL spectra of interlayer and intralayer excitons in macroscopic MoSe₂/WSe₂ heterobilayers and monolayers exfoliated onto SiO₂ without h-BN encapsulation. Black and grey: AA- and AB-stacked MoSe₂/WSe₂ hetero bilayer; blue: MoSe₂ monolayer; red: WSe₂ monolayer. All samples were exfoliated onto oxide terminated silicon passivated by a hydrophobic self-assembled monolayer. (38) We used commercial CVT grown MoSe₂ and WSe₂ crystals. The use of low-quality CVT crystals and the absence of h-BN encapsulation are both responsible for the much broader PL emission peaks than those in Fig. 4 and Fig. S8.

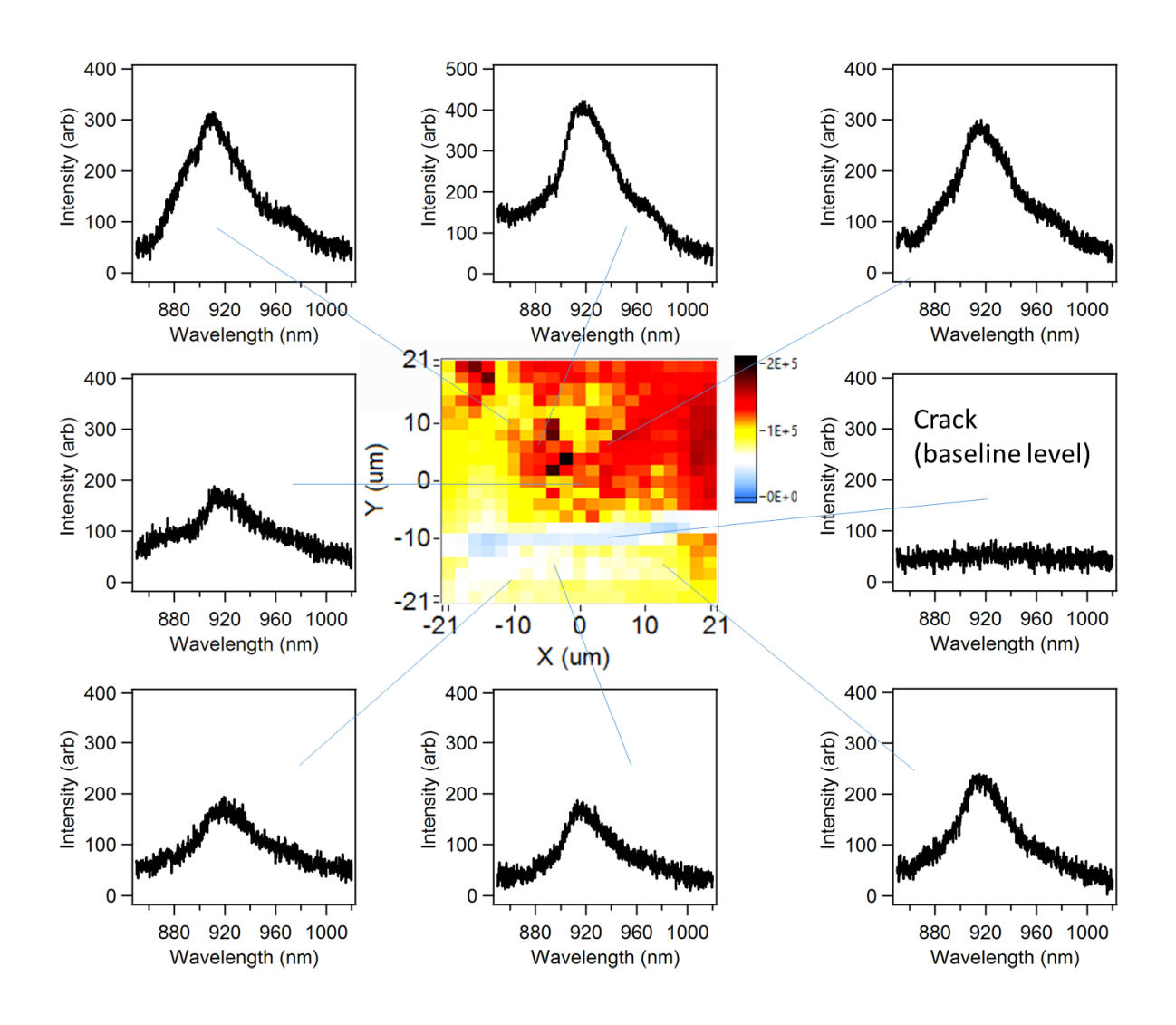


Figure S10. Low temperature (4K) PL spectra and intensity mapping of interlayer excitons from the macroscopic $MoSe_2/WSe_2$ heterostructure on SiO_2/Si substrate over a 40 μm x 40 μm area. The area is selected with a crack in the center to show the baseline level in detection. The use of low-quality CVT crystals and the absence of h-BN encapsulation are both responsible for the much broader PL emission peaks than those in Fig. 4c and Fig. S8. The intensity variation across the $40x40~\mu m^2$ area in the 2D pseudocolor plot is only \sim a factor of two, except for the crack.